Unifying Optical Selection Rules for Excitons in Two Dimensions: Band Topology and Winding Numbers

Ting Cao, Meng Wu, and Steven G. Louie

Phys. Rev. Lett. **120**, 087402 — Published 23 February 2018

DOI: 10.1103/PhysRevLett.120.087402

Unifying Optical Selection Rules for Excitons in Two Dimensions: Band Topology and Winding Numbers

Ting Cao+, Meng Wu+, and Steven G. Louie*

Department of Physics, University of California at Berkeley, Berkeley, California 94720, USA, and Materials Sciences Division, Lawrence Berkeley National Laboratory, Berkeley, California 94720, USA.

* sglouie@berkeley.edu

Abstract:

We show that band topology can dramatically change the photophysics of two-dimensional (2D) semiconductors. For systems in which states near the band extrema are of multi-component character, the spinors describing these components (pseudospins) can pick up nonzero winding numbers around the extremal k-point. In these systems, we find that the strength and required light polarization of an excitonic optical transition are dictated by the *optical matrix element* winding number, a unique and heretofore unrecognized topological characteristic. We illustrate these findings in three gapped graphene systems – monolayer graphene with inequivalent sublattices and biased bi- and tri-layer graphene, where the pseudospin textures manifest into nontrivial optical matrix element winding numbers associated with different valley and photon circular polarization. This winding-number physics leads to novel exciton series and optical selection rules, with each valley hosting multiple bright excitons coupled to light of different circular polarization. This valley-exciton selective circular dichroism can be unambiguously detected using optical spectroscopy.

An exciton in a semiconductor is an excited state with an electron-hole pair bound by their mutual Coulomb interaction [1]. Owing to the similarity between the electron-hole binding in a semiconductor and electron-proton binding in a hydrogen atom, the hydrogenic model and their variants (for example, including electron-hole-separation dependent screening effects) are usually adopted in describing excitons in various dimensions, when the electron-hole correlation length of the exciton of interest is large compared to the unit cell size. Within this picture, the envelope functions of the excitonic states are hydrogen-like wavefunctions with even or odd parity and characterized by a series of quantum numbers. In linear optical spectroscopy, an exciton may be created or annihilated by absorbing or emitting a photon, respectively. Such coupling is allowed if the full many-body excitonic states have different parity from the ground state (these states are called optically active or bright excitons). For conventional semiconductors in which the electron (hole) states in the conduction (valence) band extreme forming the exciton are of single orbital character, this parity law together with the hydrogenic picture leads to the well-known optical selection rules: in dipole-allowed materials (e.g., GaAs, monolayer transition metal dichalcogenide, etc.), *s*-like excitons are optically active, whereas *p*-like excitons are optically inactive [1-5]. In dipole-forbidden materials (e.g., Cu_2O), the optically active excitons are *p*-like states, while *s*-like states are optically inactive [5, 6].

However, for many reduced-dimensional systems of current interest, the states near the band extrema are of multiple orbital and spin components, and the bands can have nontrivial topological characteristics. Such nontrivial topological bands may be characterized by the behavior of the amplitudes of the components that compose a band state, viewed as a multi-component spinor (the pseudospin) in **k**-space. The pseudospins of the electron and hole states can develop a complex texture with respect to the crystal momentum ($\boldsymbol{k}$) around the band extrema [7-12]. The pseudospin texture (viewed as a spinor field of $\boldsymbol{k}$) could in principle affect the energy levels, optical selection rules, and many other properties of the excitons. Recent studies have shown that Berry curvature flux leads to a fine energy-level splitting of otherwise doubly degenerate hydrogenic $2p$ excitons in monolayer transition metal dichalcogenides [13, 14]. Yet, it remains unexplored whether central properties such as the optical selection rules are altered in materials with topological band characteristics.

We show here that the conventional optical selection rules, referencing to the exciton envelope functions, are *not* valid for systems with nontrivial band topology; they need to be distinctly replaced, incorporating topological effects. In the important class of 2D materials in which the pseudospins of states near the band extrema gain a nonzero winding number (topological invariant) as the carrier adiabatically traverses around the extremal **k**-point (e.g., the K or K' valley in gapped graphene systems), a highly unconventional exciton series appears and exhibits novel valley-dependent optical selection rules and other photo-activities.

The exciton energies and wavefunctions in a semiconductor may be obtained from the solutions of the Bethe-Salpeter equation (BSE) of the interacting two-particle Green's function [15]:

$$A_{\boldsymbol{k}}^{S}\left(E_{c,\boldsymbol{k}}-E_{v,\boldsymbol{k}}\right)+\Sigma_{\boldsymbol{k}'}A_{\boldsymbol{k}'}^{S}\left\langle cv,\boldsymbol{k}\middle|\widehat{K}^{eh}\middle|cv,\boldsymbol{k}'\right\rangle=A_{\boldsymbol{k}}\Omega^{S}, \tag{1}$$

where $E_{c,\boldsymbol{k}}$ and $E_{v,\boldsymbol{k}}$ are quasiparticle energies of an electron in the conduction band and negative of the quasiparticle energy of a hole in the valence band, $A_{\boldsymbol{k}}$ describes the **k**-space exciton envelope function, and $|cv,\boldsymbol{k}\rangle$ corresponds to a free electron-hole pair (a non-interacting interband transition state) at the point $\boldsymbol{k}$ in the Brillouin zone (BZ). $\widehat{K}^{eh}$ is the electron-hole interaction kernel, containing a direct electron-hole attractive screened Coulomb term and a repulsive exchange bare Coulomb term. Ω^{S} is the excitation energy of the exciton eigenstate $|S\rangle$. For notational simplicity, we only consider here a single conduction and a single valence band. Generalization to the multiband case is straightforward, and our explicit *ab initio* results given below were performed with multiple valence and conduction bands.

The eigenstate of exciton S is a coherent superposition of free electron-hole pairs at different **k** points, and is denoted by $|S\rangle=\Sigma_{\boldsymbol{k}}A_{\boldsymbol{k}}^{S}|cv,\boldsymbol{k}\rangle$. The oscillator strength that relates to the intensity for optical transition to exciton S is given by [1, 5, 15, 16],

$$\mathrm{I}_{e}^{S}=\frac{2\left|\Sigma_{\boldsymbol{k}} A_{\boldsymbol{k}}^{S} \boldsymbol{e} \cdot\left\langle\phi_{c, \boldsymbol{k}}|\widehat{\boldsymbol{p}}| \phi_{v, \boldsymbol{k}}\right\rangle\right|^{2}}{\Omega^{S}}, \tag{2}$$

where $\boldsymbol{e}$ is the photon polarization unit vector, and $\langle\phi_{c,\boldsymbol{k}}|\widehat{\boldsymbol{p}}|\phi_{v,\boldsymbol{k}}\rangle$ the interband optical matrix element between the conduction band state $|\phi_{c,\boldsymbol{k}}\rangle$ and valence band state $|\phi_{v,\boldsymbol{k}}\rangle$.

Although the exciton energies and oscillator strengths are physical observables and thus gauge-invariant, the individual components in Eq. 2 (the exciton envelope functions in **k**-space and the interband optical matrix elements) may separately look different depending on a chosen gauge. This ambiguity arises because $|cv,\boldsymbol{k}\rangle$ could have an arbitrary phase, which would be canceled out by the complex conjugate of the same phase in $A_{\boldsymbol{k}}$. This gauge arbitrariness can be eliminated by requiring $A_{\boldsymbol{k}}$ of the lowest energy *s*-like excitonic state to be that of a hydrogen-like *s* orbital. Under this well-defined and smooth gauge, we find that an analysis of Eq. 2 illuminates clearly the physical role of the exciton envelope function and of the topological characteristics of the interband optical matrix elements in optical transitions. In dipole-allowed conventional semiconductors, the interband optical matrix elements are nearly a constant around the extremal **k**-point [1, 5]. Therefore, only *s*-like excitons have non-zero oscillator strength, as its envelope function in **k**-space is isotropic in phase (i.e., no phase winding around the extremal **k**-point).

Having topologically nontrivial bands in 2D with associated pseudospin texture of nonzero winding numbers will lead to both magnitude and phase modulations of the interband optical matrix elements with $\boldsymbol{k}$, represented by a 2D vector field with a certain winding pattern. To illustrate this effect, we decompose the interband optical matrix element $\langle\phi_{c,\boldsymbol{k}}|\widehat{\boldsymbol{p}}|\phi_{v,\boldsymbol{k}}\rangle$ into the two irreducible cylindrical components, $p_{\boldsymbol{k}+}=\boldsymbol{e}_{+}\cdot\langle\phi_{c,\boldsymbol{k}}|\widehat{\boldsymbol{p}}|\phi_{v,\boldsymbol{k}}\rangle$ and $p_{\boldsymbol{k}-}=\boldsymbol{e}_{-}\cdot\langle\phi_{c,\boldsymbol{k}}|\widehat{\boldsymbol{p}}|\phi_{v,\boldsymbol{k}}\rangle$, which correspond to coupling to left- and right-circularly polarized photon modes (σ_{-} and σ_{+}), respectively. For topologically nontrivial bands, as illustrated below, $p_{\boldsymbol{k}+}$ and $p_{\boldsymbol{k}-}$ are typically non-zero (except possibly at the extremal **k**-point), and can be viewed as two vector fields that may differ in their winding patterns. (The interband optical matrix elements $p_{\boldsymbol{k}\pm}$ are complex quantities determined by the band states and independent of the specific excitonic states.)

We shall show that the transition strength (brightness) and the specific light polarization needed for an excitonic optical transition are dictated by the phase winding of the exciton envelope function and that of the interband optical matrix elements. For an excitonic state of which the **k**-space envelope function $A_{\boldsymbol{k}}$ is a highly localized function around an extremal **k**-point (Wannier excitons), $A_{\boldsymbol{k}}$ and $p_{\boldsymbol{k}\pm}$ in the relevant small part of the BZ are dominated by a cylindrical angular phase dependence of $\sim e^{im\theta_{\boldsymbol{k}}}$ and $e^{il_{\pm}\theta_{\boldsymbol{k}}}$, respectively ($\theta_{\boldsymbol{k}}$ is the angle $\boldsymbol{k}$ made with respect to the x-axis) [1, 5]. Here, and in subsequent discussion, we shall define $\boldsymbol{k}$ as the wavevector measured from the extremal **k**-point. Thus, m is cylindrical angular quantum number of the exciton envelope function and $l_{\pm}$ are the winding numbers of $p_{\boldsymbol{k}\pm}$. From Eq. 2, the oscillator strength for an optical transition to an excitonic state S by $\sigma_{\pm}$ photon is

$$\mathrm{I}_{\sigma_{\pm}}^{S} = \frac{2\left|\Sigma_{\boldsymbol{k}} f(|\boldsymbol{k}|) e^{i(m+l_{\mp})\theta_{\boldsymbol{k}}}\right|^{2}}{\Omega^{S}}, \tag{3}$$

where $f(|\boldsymbol{k}|)$ is the radial part in the summation. $\mathrm{I}_{\sigma_{\pm}}^{S}$ is thus non-zero *only* when $m = -l_{\mp}$.

This set of selection rules is distinctly different from that in conventional semiconductors. For a system with discrete n-fold rotational symmetry, the general selection rule is:

$$m = -l_{\mp} \ (\mathrm{mod}\, n). \tag{4}$$

(A generalization to systems with discrete rotational symmetries is given in the Supplementary Information Section I.) As a result, excitons with different angular quantum numbers (i.e., different m) would couple differently to $p_{\boldsymbol{k}+}$ and $p_{\boldsymbol{k}-}$, causing multiple bright excitons each accessible by σ_{-} or σ_{+} photons. We note that Eq. 4 thus incorporates and generalizes the conventional selection rules for Wannier excitons to all 2D semiconductors.

An ideal set of materials to illustrate the predicted novel excitonic physics is the gapped graphene systems, in which a bandgap and a layer-number-dependent pseudospin texture emerge from an induced broken inversion symmetry that may be tuned. We consider three (already experimentally achieved) systems based on 1 to 3 layers of graphene [17-20]. For monolayer graphene, inversion symmetry is broken by placing the graphene layer on top of a monolayer of hexagonal boron nitride. (Details in Supplementary Information Section II). For bilayer (in a Bernal stacking order) and trilayer graphene (in a rhombohedral stacking order), inversion symmetry is broken by applying an external electric field along the out-of-plane direction. In our *ab initio* GW-BSE calculations presented below, the applied electric field was set to 0.13 eV/Å, an experimentally studied value [19]. Modifying the applied electric field strength, which determines the size of the induced bandgap, does not change the physics discussed here.

For the gapped graphene systems studied, density functional theory (DFT) calculations are performed within the local density approximation (LDA) formalism using the Quantum ESPRESSO package [21] to determine their ground-state properties. First-principles GW [22] and GW-BSE [15] methods are employed to calculate the quasiparticle band structure and excitonic states, respectively, using the BerkeleyGW package [16]. (Details in Supplementary Information Section II.)

The gapped graphene systems of 1, 2, and 3 atomic layers studied have GW quasiparticle bandgaps of 130 meV, 159 meV, and 185 meV [Fig. 1(a-c)], respectively. These values are much larger than their corresponding DFT-LDA Kohn-Sham bandgaps of 62 meV, 90 meV and 118 meV, respectively, owing to electron self-energy effects. For biased bilayer and trilayer graphene, the top valence and bottom conduction bands at the K and K' valleys develop a Mexican-hat-like shape. The pseudospin texture of the states in bilayer graphene is schematically shown in Fig. 1d, where the amplitude of the carbon π orbitals develop a phase winding around the band extremum [23].

The very different pseudospin texture of the bands in the three gapped graphene systems gives a strong layer-number and valley-index dependent interband optical matrix element winding pattern for each. We show in Fig. 2 the winding pattern of $p_{\boldsymbol{k}+}$ and $p_{\boldsymbol{k}-}$ in the K valley, defined using the gauge procedure as describe above. In the plot, the complex quantity $p_{\boldsymbol{k}+}$ or $p_{\boldsymbol{k}-}$ (which is given by a magnitude and a phase $\phi_{\boldsymbol{k}}$) are represented by an arrow with its length proportional to the magnitude and its orientation pointing along the direction with angle $\phi_{\boldsymbol{k}}$ to the *x*-axis. In monolayer graphene with inequivalent A/B sublattices [Fig. 2a, b], $p_{\boldsymbol{k}+}$ is nearly constant in magnitude and phase (arrows with constant length and orientation) and has a winding number = 0 for any contours enclosing K, whereas $p_{\boldsymbol{k}-}$ is much smaller in magnitude and its phase (the orientation of the arrows) winds clockwise around the K point twice after completing any contour enclosing K (winding number = -2). This analysis, making use of the selection rules deduced above, predicts an optically active *s* exciton series, as well as a weakly active *d* exciton series. In biased bilayer graphene, the pseudospin texture [Fig. 1d] leads to a winding number = 1 for the interband optical matrix element $p_{\boldsymbol{k}-}$ [Fig. 2e]. Compared with $p_{\boldsymbol{k}-}$, $p_{\boldsymbol{k}+}$ is much smaller in magnitude [Fig. 2d], but remains constant in both magnitude and phase around the K point (winding number = 0). We therefore predict: (i) unlike the case of gapped monolayer graphene, the *p* exciton series is now optically very active; (ii) the *s* exciton series are still somewhat optically active, but having a much smaller oscillator strength than the *p* exciton series; and (iii) importantly, the photo-excitation of the *s* excitons and *p* excitons at a given valley (K or K') requires opposite circular polarization in biased bilayer graphene. The interband optical matrix elements in biased trilayer graphene have even more features [Fig. 2g, h], leading to a winding number of 1 and 2 for $p_{\boldsymbol{k}+}$ and $p_{\boldsymbol{k}-}$, respectively, at the K valley. (Details in Supplementary Information Section III.) The 1*s* exciton envelope functions of the three gapped graphene systems studied are shown in Fig. 2c, f, and i. Our new selection-rule predictions based on topological effects are completely borne out by our explicit GW-BSE calculations of the optical absorption spectra.

The physics of interband optical matrix element winding thus leads to novel exciton series in the gapped graphene systems, with each valley hosting multiple optically active excitons whose creation requires different circular polarization. We show in Fig. 3 the calculated energy levels, required circular polarization, and oscillator strength of the first six lowest-energy excitons in the K- and K'-valley of each system. The calculated binding energies of the lowest energy exciton state of the 1-, 2-, and 3-layer systems are 34 meV, 52 meV, and 45 meV, respectively. In gapped monolayer graphene with inequivalent sublattices [Fig. 3a], as expected, the *s*-like excitons are optically bright. The 1*s* exciton in the K and K' valleys can be selectively excited by σ_- and σ_+ light, respectively, similar to monolayer transition metal dichalcogenides [24-28]. In biased bilayer graphene [Fig. 3b], however, the optically most active exciton becomes a 2*p* state that is located at 13 meV above the lowest energy 1*s* state, with an oscillator strength ~ 20 times larger than that of the $1s$ exciton. Moreover, the circular polarization for excitation of the $2p$ state is opposite to that of the $1s$ state, a feature that is directly predicted from the interband optical matrix element winding patterns depicted in Fig. 2d and Fig. 2e. In the biased trilayer graphene [Fig. 3c], the lowest energy $1s$ exciton is optically inactive from the matrix element winding patterns in Figs. 2g and 2h. Due to a significant deviation of the band dispersion from a parabola, we are no longer able to associate the higher energy excitonic states with a clear principal quantum number. However, a pair of nearly degenerate excitons with p-like and d-like orbital characters could still be identified, located at ~ 9 meV above the $1s$ state. They are excitable with σ_+ polarized light, and couple strongly (optically bright) to the ground state via $\boldsymbol{p}_{\boldsymbol{k}-}$ in Fig. 2h, either directly or through a trigonal warping effect. (There is also a weakly active p-like exciton at ~ 4 meV above the $1s$ state. Details in Supplementary Information Section III.) In all three cases, the circular polarization for excitation of every bright exciton in the K'-valley is opposite to that of a degenerate-in-energy counterpart in the K-valley due to time-reversal symmetry.

We now show how our predicted novel 2D excitonic physics may be experimentally verified by polarization-resolved optical spectroscopy. As phonon-assisted intravalley exciton energy relaxation is much more efficient than phonon-assisted intervalley exciton energy relaxation [25, 29-31], optically created excitons in one valley will predominantly relax to the lowest energy exciton in the same valley (details in Supplementary Information Section IV). Taking biased bilayer graphene as an example, resonant σ_- excitations of the K-valley $1s$ exciton will induce a σ_- photoluminescence from the excited excitons themselves, whereas resonant σ_- excitations of the K'-valley $2p$ exciton will induce photoluminescence from the K'-valley $1s$ exciton following energy relaxation from the $2p$ state to the $1s$ state. As the optical circular polarization associated with the $1s$ exciton is opposite to that of the $2p$ exciton in the same valley [Fig. 3b], the latter excitations would produce a σ_+ photoluminescence. This predicted new phenomenon in biased bilayer graphene is distinctly different from the behavior of photoluminescence in monolayer transition metal dichalcogenides or gapped monolayer graphene [24-27], because the circular polarization of the luminescence light for the former would depend not only on the polarization of the incident light, but also on the excitation energy (i.e., whether it is in the range of the 1*s* or 2*p* exciton energy).

In summary, we have presented the discovery of a set of new unifying optical selection rules as well as results of novel exciton series arising from band topological effects in 2D semiconductors. All 2D systems, with or without nontrivial band topology, have optical selection rules given by Eq. 4 replacing the conventional ones for Wannier excitons. Owing to the Poincaré–Hopf theorem, which in the present context states that the sum of the winding numbers from all band extrema in the 2D BZ should equal to zero (the Euler characteristics of a 2D torus), one should look for manifestations of nonconventional selection rules in the excitonic spectra of multi-valley 2D materials. Our work reveals another important manifestation of band topology in the physical properties of materials; it also open opportunities for use of these effects in gapped graphene systems for potential valleytronic applications.

Acknowledgments:

This work was supported by the van der Waals Heterostructures Program at the Lawrence Berkeley National Lab through the Office of Science, Office of Basic Energy Sciences, U.S. Department of Energy under Contract No. DE-AC02-05CH11231. Supported by the National Science Foundation under Grant No. DMR-1508412 is also acknowledged, which provided for the GW calculations. Computational resources were provided by the DOE at Lawrence Berkeley National Laboratory's NERSC facility and the NSF through XSEDE resources at NICS. We thank L. J. and F. W. for helpful discussions.

[+] T. C. and M. W. contribute equally to this work.

Figures

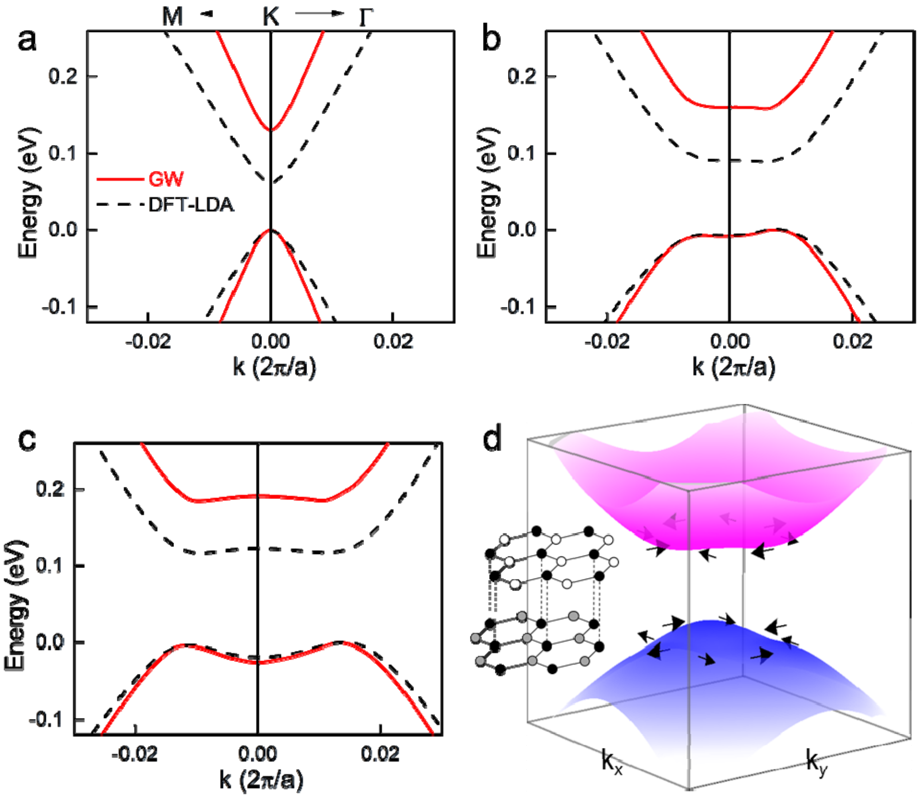

FIG. 1. Calculated band structure and orbital phase winding of gapped graphene systems. Bottom conduction band and top valence band of monolayer graphene with broken A/B sublattice symmetry (a), biased Bernal-stacked bilayer graphene (b), and biased rhombohedral-stacked trilayer graphene (c). Red solid lines and black dashed lines are GW and DFT-LDA bands, respectively. The K point is set at k = 0. Positive and negative k values denote the K-Γ and K-M direction, respectively. (d) Orbital pseudospin phase winding in biased bilayer graphene. Inset: structure of biased bilayer graphene. The carbon atoms forming bonds with a neighboring layer are colored black.

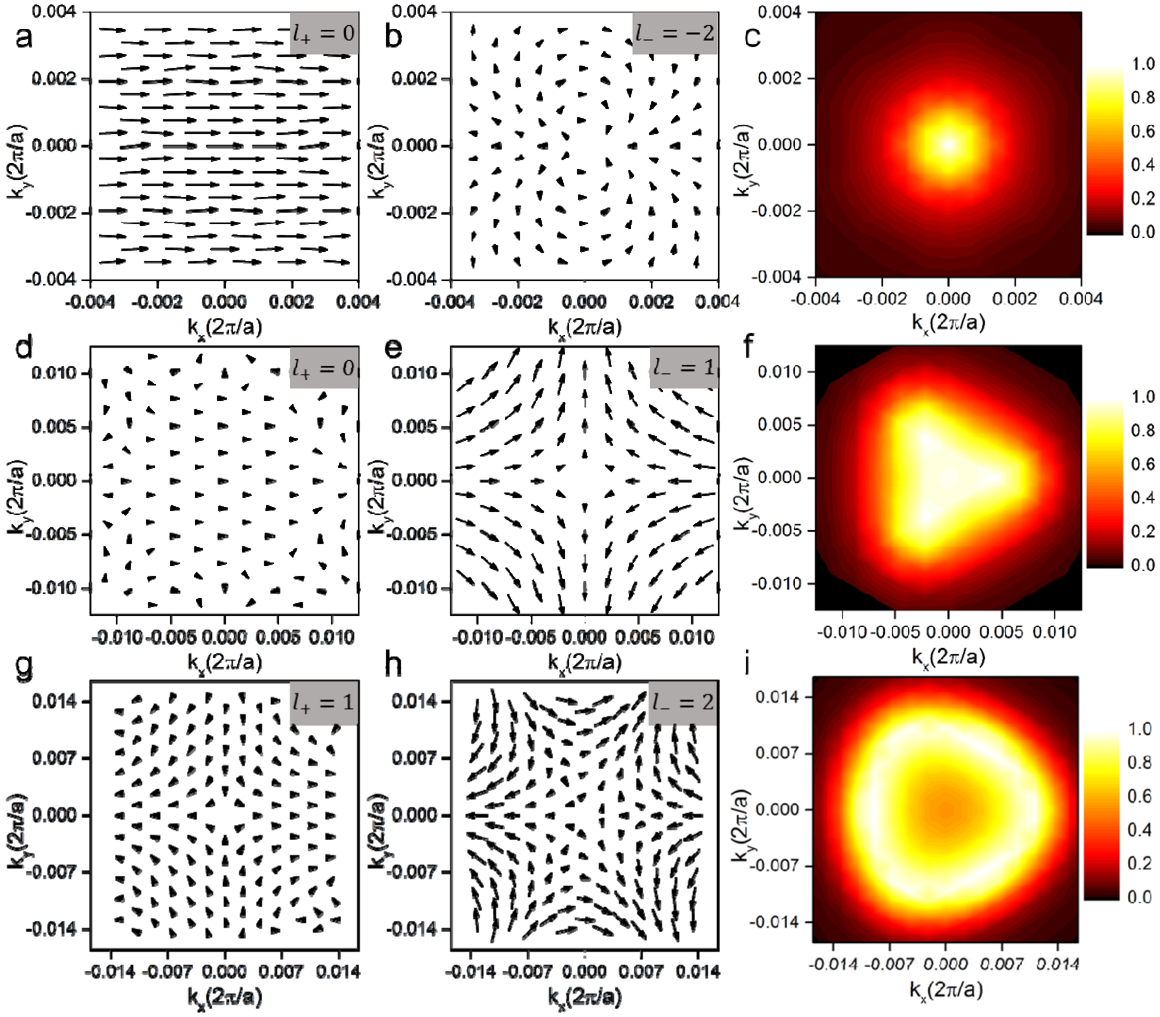

FIG. 2. K-valley interband optical transition matrix elements and 1*s* exciton envelope function in **k**-space. The K point is placed at the origin. Optical interband transition matrix element and its winding number for light of (a) left circular polarization $p_{\mathbf{k}+}$ and (b) right circular polarization $p_{\mathbf{k}-}$ in monolayer graphene with inequivalent sublattices. The direction and length of an arrow denote respectively the phase and the magnitude of the corresponding matrix element. (d) $p_{\mathbf{k}+}$ and (e) $p_{\mathbf{k}-}$ in biased bilayer graphene. (g) $p_{\mathbf{k}+}$ and (h) $p_{\mathbf{k}-}$ in biased trilayer graphene. (c, f, i) 1*s* exciton envelope function in **k**-space in gapped monolayer graphene, biased bilayer graphene, and biased trilayer graphene, respectively. The envelope functions show the magnitude of the free electron-hole pair excitation at each **k**, normalized to its largest value in each plot.

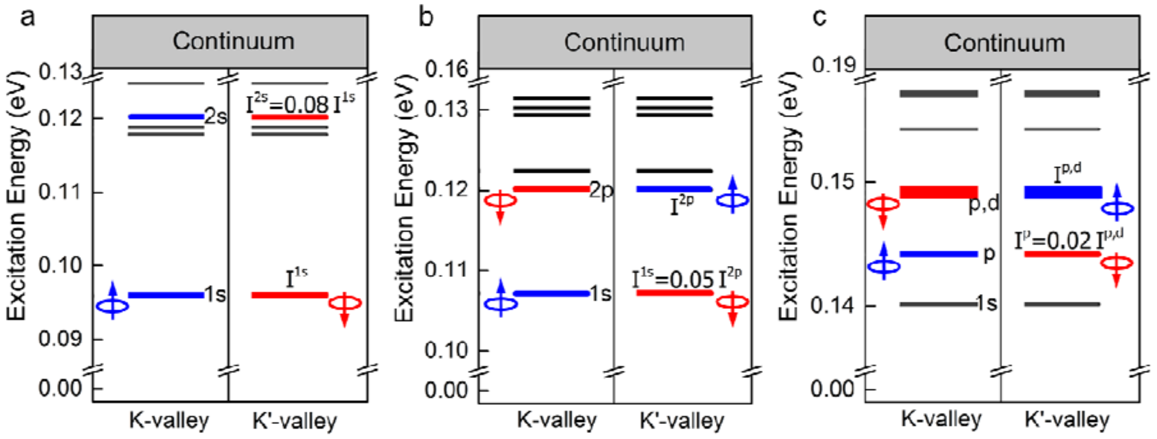

FIG. 3. K-valley and K’-valley exciton energy levels and valley-exciton selective circular dichroism in (a) monolayer graphene with inequivalent A/B sublattices, (b) biased bilayer graphene, and (c) biased trilayer graphene. Left (right) part of each panel depicts the K-valley (K’-valley) exciton energy levels. The first six lowest-energy excitons are shown in each plot. Black lines indicate dark states (with maximum oscillator strength < 1% of the brightest exciton in each plot). The oscillator strength (I) of each bright state is expressed in terms of that of the brightest state, for unpolarized light. Blue and red lines (or circles) indicate bright states with left and right optical circular polarization, respectively.

References

[1] M. L. Cohen and S. G. Louie, *Fundamentals of Condensed Matter Physics* (Cambridge University Press, 2016).
[2] A. Chernikov, T. C. Berkelbach, H. M. Hill, A. Rigosi, Y. Li, O. B. Aslan, D. R. Reichman, M. S. Hybertsen, and T. F. Heinz, Phys. Rev. Lett. **113**, 076802 (2014).
[3] K. He, N. Kumar, L. Zhao, Z. Wang, K. F. Mak, H. Zhao, and J. Shan, Phys. Rev. Lett. **113**, 026803 (2014).
[4] Z. Ye, T. Cao, K. O'Brien, H. Zhu, X. Yin, Y. Wang, S. G. Louie, and X. Zhang, Nature (London) **513**, 214 (2014).
[5] R. J. Elliott, Phys. Rev. **108**, 1384 (1957).
[6] E. F. Gross, Nuovo Cimento **Suppl. 3**, 672 (1956).
[7] M. Z. Hasan and C. L. Kane, Rev. Mod. Phys. **82**, 3045 (2010).
[8] X.-L. Qi and S.-C. Zhang, Rev. Mod. Phys. **83**, 1057 (2011).
[9] E. McCann and M. Koshino, Rep. Prog. Phys. **76**, 056503 (2013).
[10] M. Sui *et al.*, Nature Phys. **11**, 1027 (2015).
[11] L. Ju *et al.*, Nature (London) **520**, 650 (2015).
[12] F. Zhang, A. H. MacDonald, and E. J. Mele, P. Natl. Acad. Sci. USA **110**, 10546 (2013).
[13] J. Zhou, W.-Y. Shan, W. Yao, and D. Xiao, Phys. Rev. Lett. **115**, 166803 (2015).
[14] A. Srivastava and A. Imamoglu, Phys. Rev. Lett. **115**, 166802 (2015).
[15] M. Rohlfing and S. G. Louie, Phys. Rev. B **62**, 4927 (2000).
[16] J. Deslippe, G. Samsonidze, D. A. Strubbe, M. Jain, M. L. Cohen, and S. G. Louie, Comput. Phys. Commun. **183**, 1269 (2012).
[17] W. Bao *et al.*, Nature Phys. **7**, 948 (2011).
[18] C. H. Lui, Z. Li, K. F. Mak, E. Cappelluti, and T. F. Heinz, Nature Phys. **7**, 944 (2011).
[19] Y. Zhang, T.-T. Tang, C. Girit, Z. Hao, M. C. Martin, A. Zettl, M. F. Crommie, Y. R. Shen, and F. Wang, Nature (London) **459**, 820 (2009).
[20] R. V. Gorbachev *et al.*, Science **346**, 448 (2014).
[21] P. Giannozzi *et al.*, J. Phys. Condens. Mater. **21**, 395502 (2009).
[22] M. S. Hybertsen and S. G. Louie, Phys. Rev. B **34**, 5390 (1986).
[23] C.-H. Park and S. G. Louie, Nano Lett. **10**, 426 (2010).
[24] T. Cao *et al.*, Nat. Commun. **3**, 1882 (2012).
[25] K. F. Mak, K. He, J. Shan, and T. F. Heinz, Nature Nanotechnol. **7**, 494 (2012).
[26] D. Xiao, G.-B. Liu, W. Feng, X. Xu, and W. Yao, Phys. Rev. Lett. **108**, 196802 (2012).
[27] H. Zeng, J. Dai, W. Yao, D. Xiao, and X. Cui, Nature Nanotechnol. **7**, 490 (2012).
[28] T. C. Berkelbach, M. S. Hybertsen, and D. R. Reichman, Phys. Rev. B **92**, 085413 (2015).
[29] J.-A. Yan, W. Y. Ruan, and M. Y. Chou, Phys. Rev. B **77**, 125401 (2008).
[30] X. D. Xu, W. Yao, D. Xiao, and T. F. Heinz, Nature Phys. **10**, 343 (2014).
[31] J. Xiao, Z. L. Ye, Y. Wang, H. Y. Zhu, Y. Wang, and X. Zhang, Light Sci. Appl. **4**, e366 (2015).